NEUROSCIENCE

INTERNATIONAL BRAIN
IBRO
RESEARCH ORGANIZATION

Endocannabinoid Signaling in Embryonic Neuronal Motility and Cell–Cell Contact – Role of mGluR5 and TRPC3 Channels

Pauli M. Turunen,[a*†] Lauri M. Louhivuori,[a†] Verna Louhivuori,[a] Jyrki P. Kukkonen [a,b] and Karl E. Åkerman [a]

[a] *Faculty of Medicine, Medicum, Division of Physiology, PO Box 63, University of Helsinki, FIN-00014 Helsinki, Finland*

[b] *Faculty of Veterinary Medicine, Department of Veterinary Biosciences, PO Box 66, FIN-00014 University of Helsinki, Finland*

Abstract—Cell–cell communication plays a central role in the guidance of migrating neuronal precursor cells during the development of the cerebral cortex. Endocannabinoids (eCBs) have previously been shown to be one of the central factors regulating neuronal migration. In this study the effects of eCBs on different parameters, expected to affect embryonic cortical neuronal motility have been analyzed in neurosphere-derived neuroblasts using time-lapse microscopy. Increased endogenous production of the endocannabinoid 2-arachidonyl glycerol (2-AG) causes bursts of neuroblast motility. The neuroblasts move longer distances and show a low frequency of turning, and the number of neuron–neuron contacts are reduced. Similar changes occur interfering with the function of the metabotropic glutamate receptor 5 (mGluR5) or its transducer canonical transient receptor potential channel 3 (TRPC3) or the neuregulin receptor ErbB4. Blocking of 2-AG production reverses these effects. The data suggest that eCB-regulated neuronal motility is controlled by mGluR5/TRPC3 activity possibly via NRG/ErbB4 signaling. © 2018 IBRO. Published by Elsevier Ltd. All rights reserved.

Key words: 2-AG, endocannabinoids, mGluR5, neuroblast, radial glia, TRPC3.

INTRODUCTION

Neuronal migration is essential for the development of the cerebral cortex. Neuronal precursor cells migrate from the ventricular walls along a path created by radial glial processes (Kriegstein and Noctor, 2004). The correct

---

*Corresponding author. Address: Biomedicum Helsinki, Faculty of Medicine, Department of Physiology, PO Box 63, FIN-00014 University of Helsinki, Finland.

E-mail address: pauli.m.turunen@helsinki.fi (P. M. Turunen).

[†] Both co-authors contributed equally to this work.

Abbreviations: 2-AG, 2-arachidonoyl glycerol; $[Ca^{2+}]_i$, intracellular free calcium concentration; Afatinib, *N*-[4-[(3-chloro-4-fluorophenyl)amino]-7-[[(3*S*)-tetrahydro-3-furanyl]oxy]-6-quinazolinyl]-4-(dimethylamino)-2-butenamide; AM251, 1-(2,4-dichlorophenyl)-5-(4-iodophenyl)-4-methyl-*N*-1-piperidinyl-1*H*-pyrazole-3-carboxamide; AMPA, α-amino-3-hydroxy-5-methyl-4-isoxazolepropionic acid; BDNF, brain-derived neurotrophic factor; DAG, diacylglycerol; DAGL, diacylglycerol lipase; DHPG, (*S*)-3,5-dihydroxyphenylglycine; ErbB, v-erb-a erythroblastic leukemia viral oncogene homolog; Gefitinib, *N*-(3-chloro-4-fluorophenyl)-7-methoxy-6-[3-(4-morpholinyl)propoxy]-4-quinazolinamine; GLAST, glutamate aspartate transporter; HBM, HEPES-buffered media; HU-210, 3-(1,1′-dimethylheptyl)-6a*R*,7,10,10a*R*-tetrahydro-1-hydroxy-6,6-dimethyl-6*H*-dibenzo[b,d]pyran-9-methanol; JZL184, 4-nitrophenyl-4-[dibenzo[d][1,3]dioxol-5-yl(hydroxy) methyl] piperidine-1-carboxylate; MAGL, monoacylglycerol lipase; MAP-2, mitogen-associated protein-2; mGluR5, metabotropic glutamate receptor 5; MPEP, 2-methyl-6-(2-phenylethynyl)pyridine hydrochloride; NPC, neural progenitor cell; NRG1, neuregulin-1; PBST, phosphate-buffered saline + 0.1% (w/w) tween-20; pyr3, ethyl-1-(4-(2,3,3-trichloroacrylamide)phenyl)-5-(trifluoromethyl)-1*H*-pyrazole-4-carboxylate; THL, *N*-formyl-ʟ-leucine (1*S*)-1-[[(2*S*,3*S*)-3-hexyl-4-oxo-2-oxetanyl]methyl]dodecyl ester; TRPC3, canonical transient receptor potential channel 3; TrkB, tyrosine receptor kinase B.

destination is ensured by attracting and repulsing external guiding cues secreted by neighboring cells (Kriegstein and Noctor, 2004). Neuronal guiding by the radial glial scaffold and neuron–neuron contacts are particularly important (Rakic et al., 2009). Migration is guided by typical chemotactic factors such as neurotrophins (e.g., brain-derived neurotrophic factor, BDNF), netrins, semaphorins and reelin (reviewed in Rao et al., 2002; Marin et al., 2010). Also neurotransmitters, via their interaction with ionotropic or metabotropic receptors, have an important role in regulating the migratory process (reviewed in Nguyen et al., 2001; Jansson and Akerman, 2014).

Endocannabinoids (eCBs), acting on G-protein-coupled CB1 and CB2 cannabinoid receptors, have been shown to have a central role in regulating neurogenesis and neuronal migration (reviewed in Galve-Roperh et al., 2009; Keimpema et al., 2011; Di Marzo, 2011; Maccarone et al., 2014). In addition, activation of the CB1 receptor has been suggested to lead to repulsion of the growth cone through rearrangement of the cytoskeleton (Berghuis et al., 2007). eCBs act as paracrine or autocrine modulators at relatively short distances ($\leqslant$100 μm). 2-arachidonoylglycerol (2-AG), the suggested main eCB in the brain, is produced on demand from diacylglycerol (DAG) by the putatively calcium-activated diacylglycerol lipase α (DAGLα) (Bisogno et al., 2003; Gao et al., 2010; Tanimura et al., 2010; reviewed in Oudin et al., 2011b; Di Marzo, 2011). It is degraded mainly by

monoacylglycerol lipase (MAGL) to arachidonic acid (reviewed in Savinainen et al., 2012). Patterned distribution and trafficking of these enzymes in the nervous systems allows generation of gradients and local hot/cold 2-AG spots (Keimpema et al., 2010; reviewed in Maccarrone et al., 2014).

The metabotropic glutamate receptor 5 (mGluR5) is also essential for normal neurogenesis (Di Giorgi Gerevini et al., 2004; Brazel et al., 2005; Gandhi et al., 2008; Jansson et al., 2013; Zhao et al., 2014; reviewed in Jansson and Akerman, 2014). We have recently shown that in a subventricular embryonic neurosphere model this receptor is predominantly expressed on radial glial-type cells (Jansson et al., 2013; Louhivuori et al., 2015). mGluR5 is coupled to activation of a nonselective cation channel, canonical transient receptor potential channel 3 (TRPC3) (Kim et al., 2003; Berg et al., 2007; Louhivuori et al., 2015), which has previously been shown to act as regulator of chemotaxis (Li et al., 1999; Amaral and Pozzo-Miller, 2007). Inhibition of the function or the expression of either mGluR5 or TRPC3 leads to detachment of neuroblasts from the radial glial processes and an increase in neuronal motility (Louhivuori et al., 2015). This indicates that the radial glial mGluR5/TRPC3 signaling is somehow, probably through diffusible ligands, limiting the motility of neuroblasts (Louhivuori et al., 2015).

In addition to the central role in postnatal precursor cell motility (Oudin et al., 2011a,b), interference with eCBs signaling have been shown to cause pyramidal cell migration defects and cortical malformations (Mulder et al., 2008; Saez et al., 2014; Diaz-Alonso et al., 2017). The aim of the present study was thus to study the role of the 2-AG in the regulation of the motility pattern of cortical embryonic neuroblasts, and the interaction between mGluR5/TRPC3 and eCB systems.

EXPERIMENTAL PROCEDURES

Cell culture and neuronal differentiation

Neuronal progenitor cells (NPCs) were isolated from the walls of the lateral ventricles of embryonic day 14.5 129SvJ/C57Bl6/N mice, as described previously (Reynolds and Weiss, 1992). Cells from this region are considered to mainly represent precursors for cortical glutamatergic neurons at embryonic day 14.5. Briefly, cells were grown as free-floating aggregates, known as neurospheres, in Dulbecco's Modified Eagle Medium: Ham's Nutrient Mixture F-12 media (1:1) containing B27 supplement (both from Gibco, Life Technologies Ltd., Paisley, UK), 2 mM L-glutamine, 15 mM 4-(2-hydroxyethyl) piperazine–1-ethanesulfonic acid (HEPES), 100 U/ml penicillin, and 100 U/ml streptomycin (all from Sigma–Aldrich, St. Louis, MO, USA), in the presence of 10 ng/ml basic fibroblast growth factor and 20 ng/ml epidermal growth factor (both from PeproTech EC Ltd, London, UK), in a humidified incubator in 5% CO_2 at +37 °C. The culture medium was changed every Monday and Friday, and growth factors were added every Monday, Wednesday, and Friday. Cells were passaged by manual trituration at approximately 7- to 10-day intervals. For neuronal differentiation, neurospheres were

plated on poly-DL-ornithine (Sigma–Aldrich, St. Louis, MO, USA)-coated culture dishes or cover glasses in the absence of mitogens. Growth factor withdrawal induced spontaneous neurosphere attachment to the dishes, extension of thick radial processes and appearance neuroblasts moving in close contact with these processes (Fig. 1A).

Drugs

4-nitrophenyl-4-[dibenzo[d][1,3]dioxol-5-yl(hydroxy) methyl] piperidine-1-carboxylate (JZL184; used at 10M), N-formyl-L-leucine (1S)-1-[[(2S,3S)-3-hexyl-4-oxo-2-oxetanyl] methyl]dodecyl ester (THL; used at 1M), ethyl-1-(4-(2,3,3-trichloroacrylamide)phenyl)-5-(trifluoromethyl)-1H-pyrazole-4-carboxylate (pyr3; used at 1M), (S)-3,5-dihydroxyphenylglycine (DHPG; used at 10M), N-[4-[(3-chloro-4-fluorophenyl)amino]-7-[[(3S)-tetrahydro-3-fur-anyl]oxy]-6-quinazolinyl]-4-(dimethylamino)-2-butenamide (afatinib/BIBW 2992; used at 0.1M), N-(3-chloro-4-fluorophenyl)-7-methoxy-6-[3-(4-morpholinyl)propoxy]-4-quinazolinamine (gefitinib; used at 4M), and 2-methyl-6-(2-phenylethynyl)pyridine hydrochloride (MPEP; used at 10M) were from Tocris Bioscience (Bristol, UK). 1-(2,4-dichlorophenyl)-5-(4-iodophenyl)-4-methyl-N-1-piperidinyl-1H-pyrazole-3-carboxamide (AM251; used at 10M) and 3-(1,1′-dimethylheptyl)-6aR,7,10,10aR-tetra hydro-1-hydroxy-6,6-dimethyl-6H-dibenzo[b,d]pyran-9-methanol (HU-210; used at 1M) were from Cayman Europe (Tallinn, Estonia) and brain-derived neurotrophic factor (BDNF; used at 10ng/ml), and neuregulin-1 (NRG1; used at 20ng/ml) from PeproTech.

Immunostaining protocol

BL6-derived neurospheres were plated on poly-L-ornithine coated (0.05 mg/ml in PBS, pH 8, 3 h, +37 °C,) glass cover slips on 24-well plate and allowed to differentiate for 3 days. The cells were fixed with 4% paraformaldehyde (Sigma) for 20 min in room temperature (RT), followed by three washing steps with PBST (PBS + 0.1% tween-20, pH 7.4, from Sigma). When needed, the cells were permeabilized with PBS + 0.5% triton X-100, pH 7.4 (Sigma) for 7 min in RT. After three washing steps with PBST, blocking for unspecific staining was done with UltraVision™ Protein Block (Thermo Fisher Scientific, Waltham, MA, USA) for 10 min in RT. Blocking solution was removed and the 1st antibody in 200 μl in PBST was added for 1 h in RT. Unbound immunoglobulins were removed by washing three times 10 min with PBST. The 2nd antibody-conjugate (Alexa Fluor 488 or Alexa Fluor 568) incubation was performed in 200 μl for 1 h in RT, followed by four 10-min washing steps. Cells were mounted with Prolong Diamond Antifade Moutant with DAPI (Thermo Fisher Scientific, Waltham, MA, USA). Antibodies and concentrations used in this study were: anti-ErbB1, 1:100 (R&D Systems/Bio-Techne Ltd. Abingdon, UK); anti-MAP-2, 1:500 (Abcam, Cambridge, UK); anti-CB₁, 1:100 (Abcam, Cambridge, UK), donkey-anti goat Alexa Fluor 568 1:500, donkey-anti mouse Alexa Fluor 568 1:500, donkey-anti rabbit Alexa Fluor
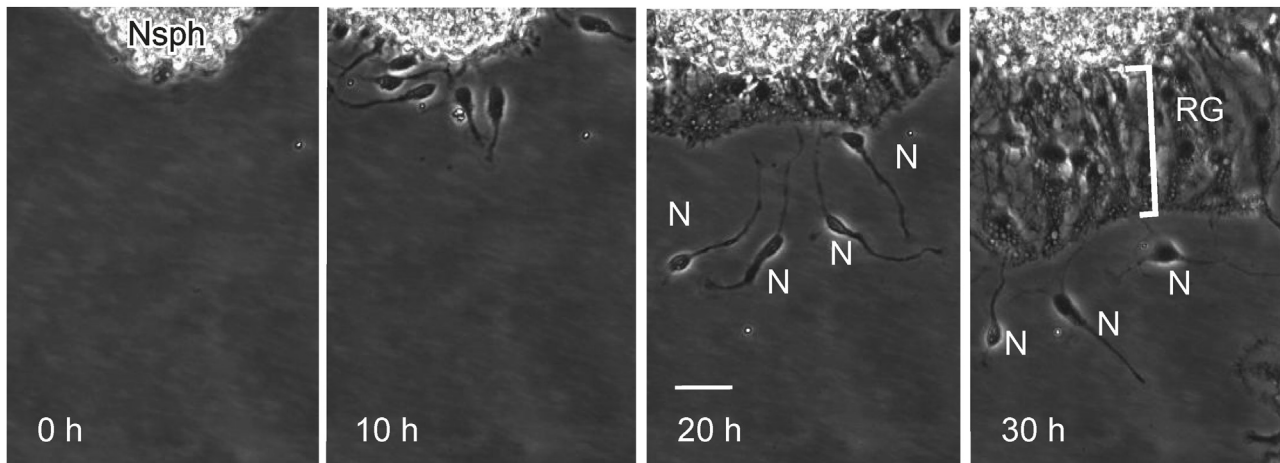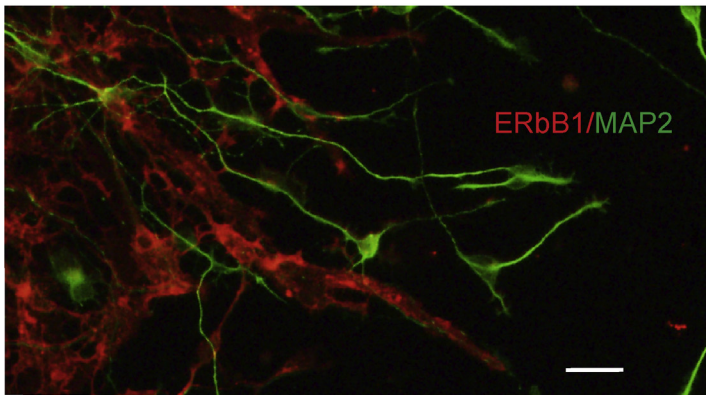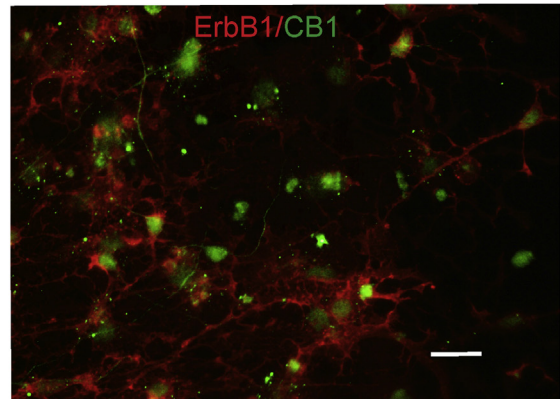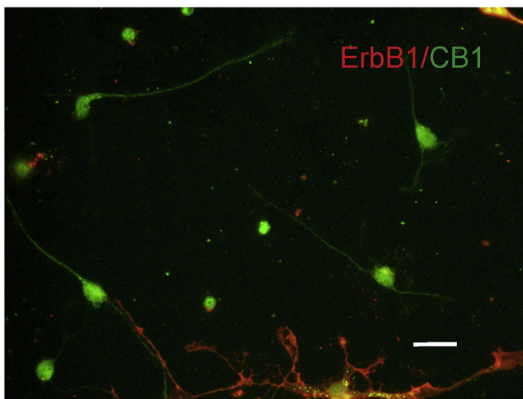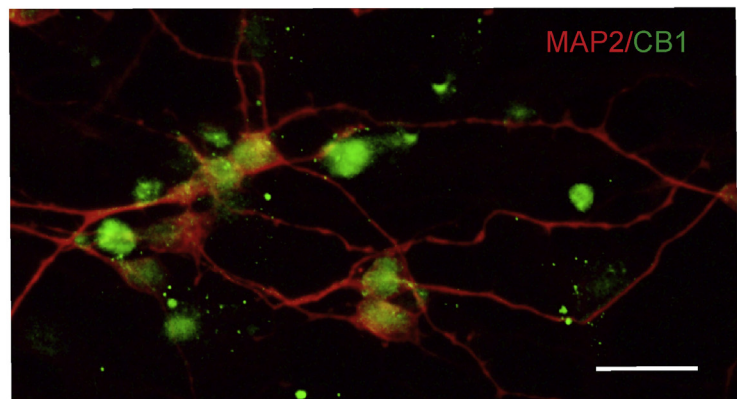
Fig. 1. The spatial distribution of neurosphere-derived cells and immunocytochemistry of CB_1 receptors. (A) Selected images from a time-lapse series showing emergence of neuroblasts from the neurosphere (Npsh). Radial glial-like cells are denoted with RG and neurons with N. (B) Immunostaining for the glial marker ErbB1 receptors and the neuronal marker MAP-2. (C, D) Immunostaining for ErbB1 and CB_1 (E). Immunostaining for MAP-2 and CB_1. The scale bar = 50 μm.

488 1:500. All 2nd antibodies were from Invitrogen, Eugene, Oregon, USA. Images were taken with Olympus AX-70 microscope and pictures were analyzed with ImageJ-software (Schneider et al., 2012).

Time-lapse imaging

Time-lapse imaging of cellular movement was performed in a self-contained cell-culturing instrument combining

phase contrast microscopy, automation and environmental control (Cell-IQ system, Chip-Man Technologies Ltd., Tampere, Finland). The imaging system enables continuous monitoring of adherent cells on two multiwall plates in an integrated plate holder. Time-lapse images were analyzed with ImageJ and its plugin MTrackerJ (Meijering et al., 2012) as described in (Louhivuori et al., 2015), and the data quantified with Microsoft Excel (Microsoft, Redmond, WA, USA) and Origin 6.0 (OriginLabCorp, Northampton, MA, USA).

Since the basic nature of movement of neuroblasts is phasic, the average speed of movement is not always an appropriate measure of cell motility. We therefore used a previously defined quantity, *motility index* (see Louhivuori et al., 2015). Moving cells were defined as cells which move at least twice at a speed of 60 μm/h during a 10-h period. Cells which did not follow this criterion were discarded from the analysis to avoid measurements of stationary cells. Briefly, the motility index was defined as the number of time points each cell moved with a speed higher than 30 μm/h divided by the number of time points the speed of the cell was below 30 μm/h:

$$\text{motility index} = \frac{t_{\text{speed} \ >30\mu\text{m/h}}}{t_{\text{speed} \ \leqslant 30\mu\text{m/h}}}$$

The average *motility index* (Figs. 2B–E and 7) for each neuroblast was calculated for a period of at least 10 h.

Changes in direction of the movement of individual neuroblast will cause a reduction in the distance to the origin (the point where migrating neuroblast first exits the neurosphere) compared to movement directly away from this point. A measure of turning (Δdirection) was thus obtained by dividing the increment of distance from origin (distance from time point B to origin − distance from time point A to origin) with the distance traveled (the measured distance between time points B and A) for every measurement (Δdirection Fig. 3B). Values of −1 and 1 are obtained for movement toward and away from the starting point, respectively, while any other deviation from a linear path will give values between 1 and −1 and are functions of the angle by which the change in direction occurs. Δdirection was then plotted for each time point (15 min) within a time period of at least 15 h for each cell. Δdirection events (Fig. 3C) were calculated by counting each deviation of Δdirection larger than 0.2 between two time points and dividing the total number of deviations with the total number of time points for each cell to obtain the number of turns per time.

Endocannabinoid production

The production of endocannabinoids was measured as described in (Turunen et al., 2012). Briefly, approximately 100 neurospheres were plated on poly-DL-ornithine-coated 6-well plates without growth factors and allowed to differentiate for 48 h. The spheres were metabolically labeled for 24 h with 0.1 μCi/ml [14C]-arachidonic acid (PerkinElmer, Waltham, MA, USA) in culture medium containing 2.4 mg/ml lipid-free BSA as the radiolabel

carrier. Prior to the experiment, the loading medium was removed and the spheres were washed three times with HEPES-buffered saline (HBS; 137 mM NaCl, 5 mM KCl, 1 mM $CaCl_2$, 1.2 mM $MgCl_2$, 0.44 mM KH_2PO_4, 4.2 mM $NaHCO_3$, 10 mM glucose, and 20 mM HEPES, adjusted to pH 7.4)/lipid-free BSA to remove residual extracellular radioactivity. The spheres were incubated with inhibitors in HBS/lipid-free BSA for 15 min at +37 °C. The experiment was stopped by transferring the plates on ice and collecting the extracellular solutions to Eppendorf tubes. Possible cellular debris was centrifuged down (2 min, 14,000g at +4 °C) to prevent contaminations originating from the membrane fraction.

For endocannabinoid detection, lipids were extracted from the supernatant with modified Bligh and Dyer method as described in (Turunen et al., 2012). Briefly, 800 μl of the supernatant was transferred to Kimax tubes (Kimble Glass Inc., Vineland, NJ, USA) containing 2 ml methanol and 1 ml chloroform. The tubes were thoroughly vortexed and additional 1 ml of chloroform and 1 ml of water were added. Tubes were mixed again and centrifuged for 5 min at 500g in room temperature to complete the phase separation. The lower, lipid-containing organic phase was then acquired and dried under N_2 stream. Samples were dissolved in chloroform and applied directly to pre-dried thin layer chromatography (TLC) plates (Silicagel 60; Merck, Darmstadt, Germany) with non-labeled lipid standards for 2-AG, anandamide and arachidonic acid (all from Cayman Chemical Company, Ann Arbor, MI, USA). The plates were developed with a running solution containing ethyl acetate: isooctane: acetic acid (144:56:20).

TLC-plates were dried and radioactivity was quantified by exposing imaging plates (BAS-MS, Fujifilm, Tokyo, Japan) overnight. For visualizing the unlabeled lipid standards, the plates were stained with iodine vapor, and scanned with Fujifilm FLA-5100 scanner; band areas and intensities were analyzed with ImageJ.

Gene expression analysis

Cell-type-specific gene expression was analyzed for our genes of interest using the output of the Bayesian generalized linear modeling tool (La Manno et al., 2016), which assigns regulated expression of a gene to one or more cell populations. The modeling tool resource code (https://github.com/linnarsson-lab/ipynb-lamanno2016) and datasets (GEO accession number: GSE76381) are publically available.

Data analysis

Statistical significance between groups was determined using Student's non-paired t-test with Bonferroni's correction for multiple comparisons. Significances are as follows: ns (not significant), $P > 0.05$; $^{*}P < 0.05$; $^{**}P < 0.01$; $^{***}P < 0.001$. The results are given as mean ± SD. The total number of cells analyzed is denoted with "n" and number of separate experiments with "N".
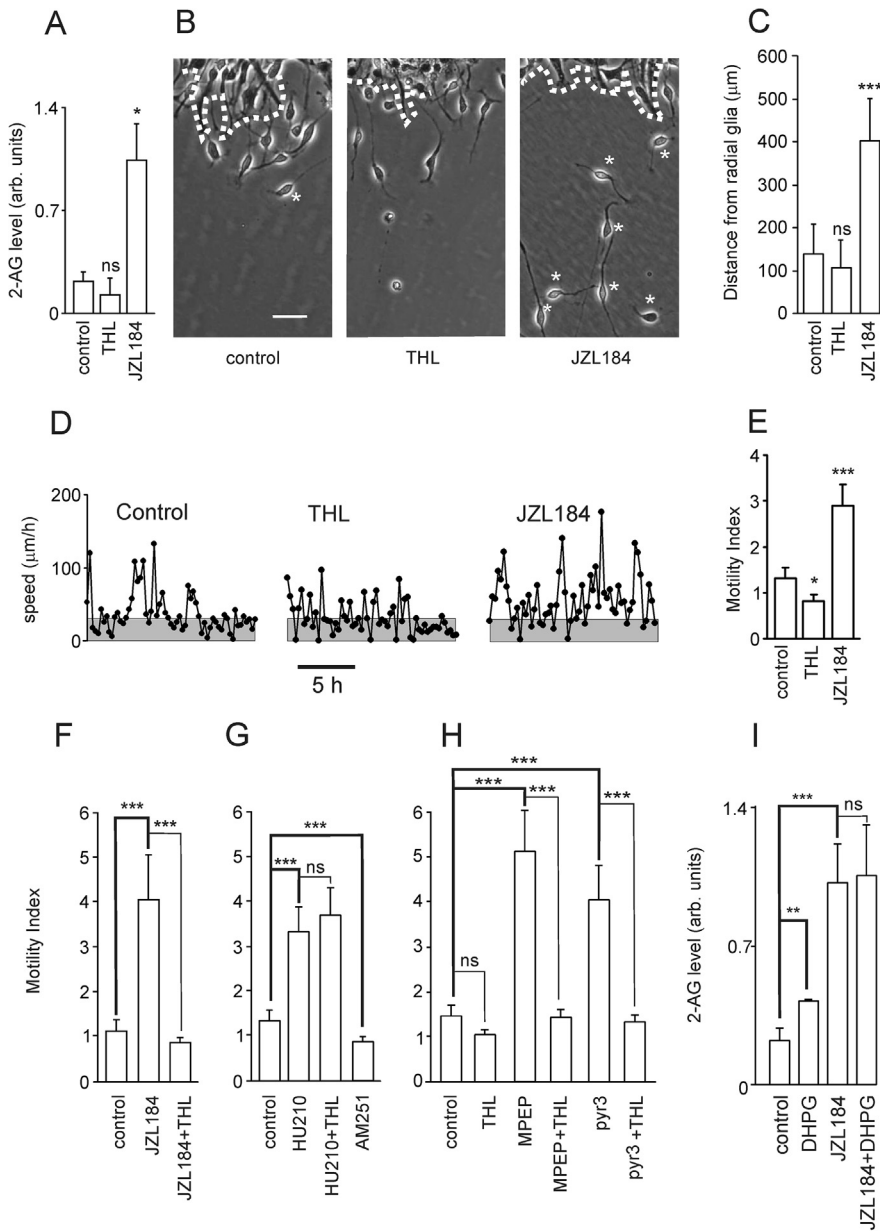
Fig. 2. The effect of 2-AG on the spatial distribution and motility of neurosphere-derived cells. (A) 2-AG levels in control cells and in cells treated with 1 μM THL and 10 μM JZL184. $N = 6$ for all treatments. (B) Examples of neuroblasts attached to radial glia or moving freely after no treatment (control) and after treatment with 1 μM THL and 10 μM JZL184. Note the close contact between neuroblasts and tips of thick radial processes (denoted with a dotted line). Neurons not attached to the radial glial layer are marked with an asterisk. Scale bar = 50 μm. (C) The maximum distance each cell had traveled from the starting point at the radial glial border. Analysis was started at 25 h from the start of the experiment and an image was analyzed every 2.5 h. Sample sizes: control cells: $n = 32$ and $N = 6$; THL-treated cells: $n = 69$, $N = 13$; and JZL184-treated cells: $n = 46$, $N = 8$. For measurements of motility images were acquired every 15 min over a time period of 48 h. Movement of single freely moving cells were tracked. (D) Speed of an individual control cell, a cell treated with 1 μM THL and a cell treated with 10 μM JZL184 is plotted as a function of time. Speed ≤ 30 μm/h is marked with gray. (E–H) Statistics of motility indices calculated from the movements of individual cells as those in (D). (E) Control cells ($n = 47$, $N = 7$) and cells treated with THL ($n = 71$, $N = 8$) and JZL184 ($n = 41$, $N = 6$). (F) Control cells ($n = 60$, $N = 10$) and cells treated with JZL184 ($n = 65$, $N = 9$), and JZL184 + THL ($n = 14$, $N = 3$). (G) Control cells ($n = 25$, $N = 5$) and cells treated with 1 μM HU-210 ($n = 53$, $N = 12$), HU-210 + THL ($n = 26$, $N = 6$) and 10 μM AM251 ($n = 52$, $N = 8$). (H) Control cells ($n = 51$, $N = 8$) and cells treated with THL ($n = 37$, $N = 8$), 10 μM MPEP ($n = 33$, $N = 6$), MPEP + THL ($n = 37$, $N = 8$), 1 μM pyr3 ($n = 28$, $N = 5$) and pyr3 + THL ($n = 40$, $N = 7$). (I) 2-AG production in the presence of 10 μM DHPG, 10 μM JZL184 and DHPG + JZL184.

RESULTS

Time-lapse imaging and immunostaining of neurosphere-derived cells for CB₁, ErbB1 and MAP-2

Endocannabinoids (eCBs) have a central role in neuronal development as paracrine messengers (Maccarrone et al., 2014) and they also increase the motility of postnatal neuronal progenitor cells (Oudin et al., 2011a). We used time-lapse microscopy to document the behavior of neurosphere-derived cells as they migrated out of the neurosphere after mitogen-removal induced differentiation. Two types of cells dominate in these cultures. Radial glial-type cells extend thick branched processes and form a dense layer (denoted RG in Fig. 1A). They are positive for the radial glial marker glutamate-aspartate transporter (GLAST), brain lipid-binding protein (BLBP) and for the mGluR5 (Jansson et al., 2013; reviewed in Jansson and Akerman, 2014). Freely moving neuroblasts are released from the radial glial layer (denoted *N* in Fig. 1A). They typically have a bipolar morphology with thin processes and stain positively for neuronal markers such as TuJ1 (class III β-tubulin), MAP-2 (microtubule-associated protein 2), NeuN (feminizing locus on X-3, Fox-3, Rbfox3, or hexaribonucleotide-binding protein-3), and ionotropic glutamate receptors (Jansson et al., 2012, 2013). Fig. 1A shows neuroblasts emerging from a neurosphere (denoted Nsph on the image) during the initial 30 h after induction of differentiation. Due to the clear difference in morphology, the cell types are distinguishable in time-lapse imaging experiments. Epidermal growth factor (EGF) is a mitogen for radial glia and some astrocytes. Calcium imaging suggests that EGF responses are seen in radial glial-type cells correlating with the responses to activation of mGluR5 (Louhivuori et al., 2018). Co-immunostaining for the EGF

receptor ErbB1 and MAP-2 shows the morphology of the two cell types (Fig. 1B). The staining for the CB_1 receptor did not appear to overlap with the staining for ErbB1 (Fig. 1C). CB_1 staining was instead detected in MAP-2-positive neuroblasts located outside the ErbB1-positive radial glial-type cells (Fig. 1D). CB_1 staining appeared to be localized to the MAP-2-positive processes (Fig. 1E).

2-AG effects on the motility index of migrating NPCs

eCBs have previously been associated with the regulation of postnatal neuronal migration (Oudin et al., 2011b). We thus wanted to assess their role in neurosphere-derived cortical embryonic neurons. We first determined the synthesis of 2-AG and anandamide, the other main eCB in the brain (Devane et al., 1992). The production of 2-AG was relatively low under basal conditions. THL (1 μM), a DAGL inhibitor, showed no significant decrease in 2-AG levels while JZL184 (10 μM), a MAGL inhibitor, caused a robust increase in 2-AG levels (Fig. 2A). Anandamide was not detected (data not shown).

The distribution of the neuroblasts with respect to their original starting position close to the radial glia processes was determined. As shown in Fig. 2B, control cells and THL-treated cells remained close to the border of radial glial processes (denoted by dotted white line), while JZL184-treated cells had moved farther out. This is

confirmed in the statistics for the maximal distance each cell had moved (Fig. 2C).

We then determined the speed over the entire measurement period for control cells, THL-treated cells, and JZL184-treated cells. The pattern of movement is shown in Fig. 2D for representative cells. As seen, the control cell moved in phases of rapid (> 100 μm/h) progression with alternating phases of slow progression or stalling (gray areas denote speed < 30 μm/h). Throughout the slow phases, the cells frequently changed direction. During this behavior, longer processes were retracted, and the cells extended short processes in many directions and rotated slowly (data not shown; see Jansson et al., 2012). These observations are in agreement with previous results on the migration pattern of subventricular zone neurons in mouse brain slices (Murase and Horwitz, 2002; Suzuki and Goldman, 2003). Note the frequent periods of stalling of the THL-treated cell (Fig. 2D). In contrast, the JZL184-treated cell stalled less frequently and showed an overall higher speed (Fig. 2D). The data were analyzed using *motility index*. THL-treatment alone caused a small reduction in the motility index, while JZL184-treatment considerably increased the *motility index* (Fig. 2E). The effect of JZL184 was completely reversed by THL (Fig. 2F). The CB_1 cannabinoid receptor agonist HU-210 (1 μM) increased the motility in a similar way as JZL184 (Fig. 2G). The HU-210-induced effect was unaffected by THL, suggesting that the effect of THL on motility is indeed due to its ability to block DAGL. The CB_1 receptor antagonist AM251 reduced the motility index (Fig. 2G) supporting the idea of intrinsic 2-AG production and CB_1 receptor activity.

The increased *motility index* measured in the presence of JZL184 is similar to the effect we have previously seen in cells in which mGluR5 receptors are inhibited with MPEP (Jansson et al., 2013), and also in cells expressing nonfunctional TRPC3 channels or TRPC3 channel are blocked with pyr3 (Louhivuori et al., 2015). We therefore wanted to determine whether inhibiting 2-AG synthesis with THL would reverse the effect of MPEP/pyr3. Addition of THL reduced the motility of both MPEP- and pyr3-treated cells to control levels (Fig. 2E). These data suggest a mechanistic link between mGluR5/TRPC3 and eCBs, i.e., reducing the signaling via the mGluR5/TRPC3 pathway appears to promote 2-AG-mediated effects on neuronal motility. AM251 also blocked the MPEP and pyr3 stimulated motility (data not shown).
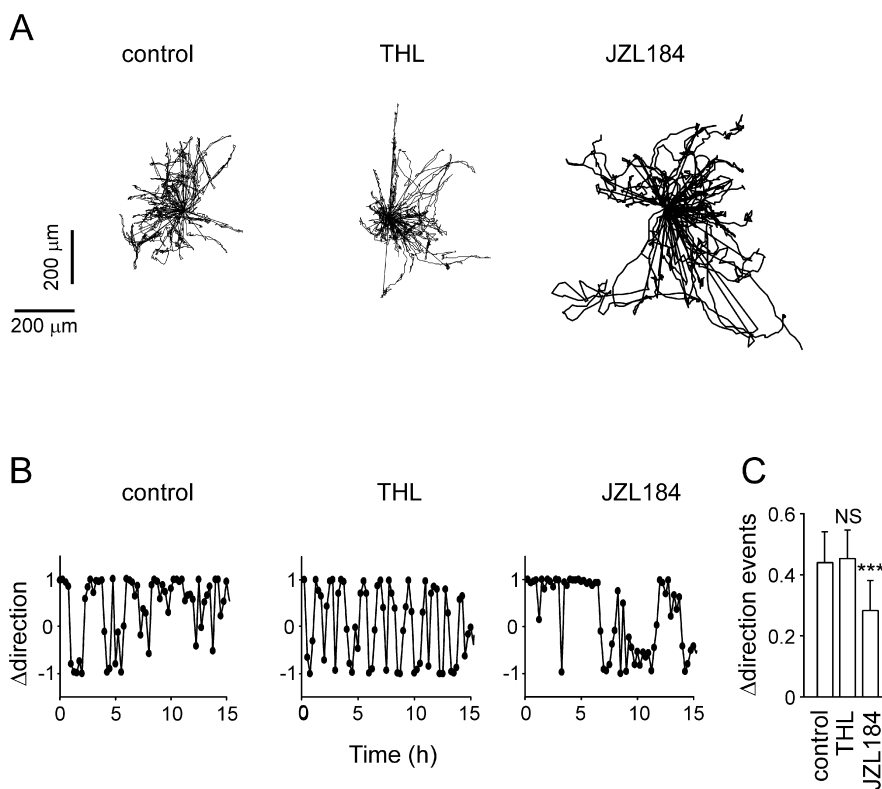

Fig. 3. The effect of 2-AG on the movement direction of neurosphere-derived neuroblasts. Images were acquired every 15 min over a time period of 48 h, and individual cells in image sequences were tracked as in Fig. 2. (A) The movement of 25 control and THL-(1 μM)- and JZL184-(10 μM)-treated cells during a time period of 15 h are superimposed. (B) The movement directions were assessed as explained under in Experimental Procedures. (C) Corresponding statistics for control ($n = 32$, $N = 6$), THL-treated ($n = 69$, $N = 13$), and JZL184-treated cells ($n = 46$, $N = 8$).

The data described above are in apparent contradiction with the expected Ca^{2+}-dependent increase in DAGL activity upon stimulation of mGluR5 (reviewed in Kano et al., 2009). We therefore tested whether stimulation of mGluR5 with DHPG would result in increased 2-AG production compared to the basal levels. DHPG doubled the 2-AG production (Fig. 2I). The DHPG-stimulated 2-AG production was, however, not further potentiated by JZL184.

Effect of 2-AG on changes in direction

The results described above indicate that eCBs act by modifying the phasic pattern of movement by promoting bursts or reducing the stalling frequency. As shown above, JZL184-treated cells moved long distances away from the radial processes. Stalling often occurs in close proximity of radial glia (Louhivuori et al., 2015) and the neuroblasts frequently change the direction of their movement after a stalling period (Jansson et al., 2012). Chemoattraction or chemorepellation changes the direction of cell movement and would be expected to affect the motility patterns. We thus determined effects of 2-AG on the spatial distribution of the cells. The distribution of 25 randomly chosen control, THL-treated and JZL184-treated cells was analyzed. As shown in Fig. 3A the control cells and THL-treated cells move close to the site of origin and seldom exceeding 200-μm distance, while JZL184-treated cells move much farther. Since a higher turning frequency limits the effective distance of migration, changes in direction of the individual cells was determined. We tracked the movement of individual cells over a time period of 15 h. The changes of direction in relation to the starting point were calculated dividing the increment of distance from origin with the distance traveled for every measurement. Representative analysis results are presented in Fig. 3B. Note the abundant turnings in control and THL-treated cells as compared to more linearly moving JZL184-treated cell, which move in a straight line away from the starting point (value 1 on y-axis). As shown in the average graph in Fig. 3C, JZL184-treated cells moved more linearly in relation to the starting point than control cells or THL-treated cells. No significant difference between control and THL-treated cells was observed.

Effect of 2-AG on the distribution of stalling cells

The data above suggest that 2-AG reduces stalling and turning events. Our previous studies suggest that diffusible substances from radial glia affect neuroblast motility in response to mGluR5/TRPC3 activity. Stalling periods frequently coincide with the interactions between the radial glial processes and the neuroblasts (Louhivuori et al., 2015). Since eCBs are diffusible with a range around 100 μm (reviewed in Maccarrone et al., 2014) we measured the number of stalling events in relation to the distance from the radial glia. An image sequence of a neuroblasts making contact with radial glial processes and finally being released after 4.5 h is shown in Fig. 4A. Note the change in the morphology at the 1
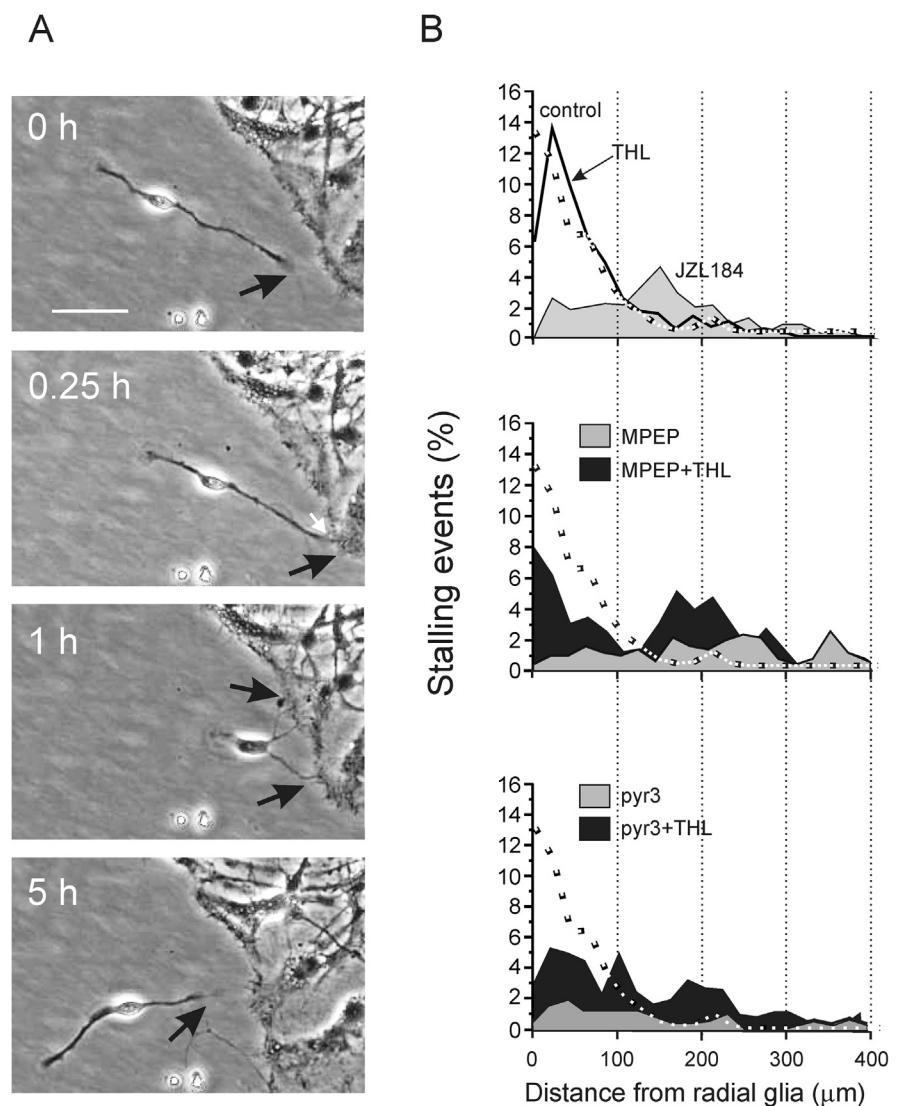

Fig. 4. The effect of 2-AG on the spatial distribution of stalling cells. (A) Selected images from a time-lapse series demonstrating a neuroblast making contact with radial processes and then being released. Scale bar = 50 μm. (B) Neuroblast stalling events (events stalled/total events × 100%) and their distances from the radial glial process in 20-μm increments under different conditions. Sample sizes: control cells: $n = 10$); THL-(1 μM)-treated cells: $n = 17$, MPEP-(10 μM)-treated cells: $n = 36$; MPEP + THL-treated cells: $n = 37$; pyr3-(1 μM)-treated cells: $n = 10$; pyr3 + THL-treated cells: $n = 29$; and JZL184-(10 μM)-treated cells: $n = 23$. The black- and white-dotted line shows the distribution of control cells. Scale bar = 50 μm.

hour time point. Fig. 4B presents the frequency distributions of the stalling events at different distances from the radial glial border. The majority of stalling (i.e., moving at speed ≤ 30 μm/h) in control and THL-treated cells was localized very close to the tips of the radial processes, and stalling cells were seldom found longer than 150 μm from the radial glia (Fig. 4B, topmost graph). Stalling events of MPEP- and pyr3-treated cells were more evenly distributed along the distances 0–400 μm from the tips of the radial processes (Fig. 4B, middle and lowermost graph). When THL was included together with MPEP or pyr3 (Fig. 4B, middle and lowermost graph), stalling was increased and the stalling cells were again positioned closer to the radial processes, mainly at a distance 0–200 μm from the tips. A population of stalling cells was found very close to the tips of the radial processes. JZL184-treated cells were distributed diffusely over long distances in a similar manner as MPEP-/pyr3-treated cells (Fig. 4B, topmost graph). Thus, both inhibition of mGluR5 and TRPC3 and elevation of 2-AG levels produce similar wide distribution of stalling cells.

Effect of 2-AG on "free cells"

Since THL only partially reversed the distribution of stalling cells during mGluR5/TRPC3 block, we wanted to investigate the effect of THL on the number of "free cells" (neuroblasts unattached to radial glia). As shown

in Fig. 5A, MPEP and pyr3 caused a significant increase in the amount of "free cells" as shown earlier (Louhivuori et al., 2015), but this change was only weakly affected by THL. MPEP and pyr3 also increased the maximum distance the cells traveled from the radial glial processes; THL only partially reversed this effect (Fig. 5B).

Effect of 2-AG on neuron–neuron interaction

As described alone, the effect of eCBs on the distribution of neuroblasts cannot be explained through an interference of neuroblasts with radial glia since THL was unable to restore the change in distribution. We noticed that interactions between neuroblasts are frequent in the image sequences. These interactions outside the radial glial layer may thus be another factor limiting their free motility. We wanted to analyze if this was indeed the reason. An image sequence of a contact between two neuroblasts is shown in Fig. 6A. The cells (contact denoted by an arrow) approach each other, attach, and finally continue migration after the contact is released. The average duration of each contact was 1.0 ± 0.4 h (calculated from 23 neurospheres). We quantified the number of contacts per total number of neuroblasts (Fig. 6B). Under control conditions the cells formed several contacts. THL-treatment alone caused a small increase in the number of contacts between cells compared to controls. MPEP and pyr3, as well as JZL184 and HU-210, significantly reduced the number of neuron–neuron contacts. THL, on the other hand, totally restored the neuron–neuron interactions in the presence of MPEP, pyr3, and even JZL184 – but not in the presence of HU-210 – suggesting that the reduction in contacts during these treatments could be mediated by intrinsic 2-AG production. We further quantified the numbers of neuron–neuron contacts along the distance to radial glial processes. In control, THL-, and JZL184-treated cells most contacts occurred 50–100 μm from nearest radial processes (Fig. 6C). The contacts seldom occurred at a distance above 200 μm.
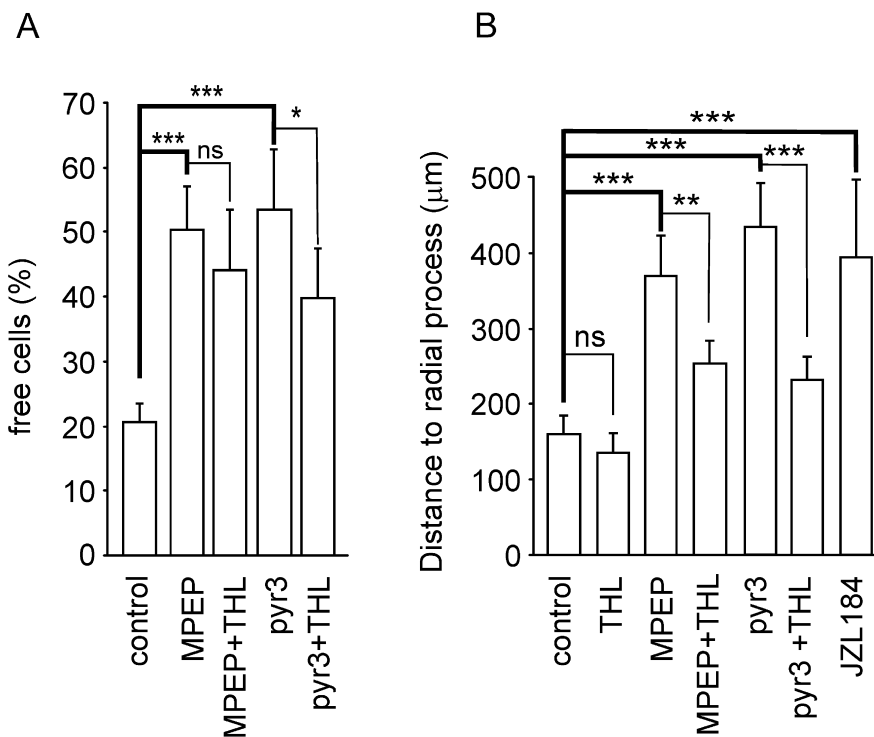
Interactions of neurotrophins and 2-AG in neuronal motility

Neuregulins, acting through the ErbB4 receptors, have been shown to play an essential role in embryonic neuronal migration (Ghashghaei et al., 2006; Rico and Marin, 2011). Likewise, BDNF promotes neuronal migration in embryonic models (Jansson et al., 2012; Zhou et al., 2015). An interaction between the eCB and the neuregulin systems is suggested by a study showing that

Fig. 5. The effect of 2-AG on the spatial distribution of stalling cells. (A) The number of unattached cells was calculated, as described in Fig. 1, for control cells and cells treated with THL (1 μM; N = 6), MPEP (10 μM; N = 4), MPEP + THL (N = 5), pyr3 (1 μM; N = 4) and pyr3 + THL (N = 6). (B) The maximum distance each cell had moved. The measurement began 25 h after the start of the experiment. Data were analyzed as described in Fig. 2. The distance of individual cells to the nearest radial glial process was determined for control cells (n = 10), THL-treated cells (n = 17), MPEP-treated cells (n = 36), MPEP + THL-treated cells (n = 37), pyr3-treated cells (n = 10), and pyr3 + THL-treated cells (n = 29).
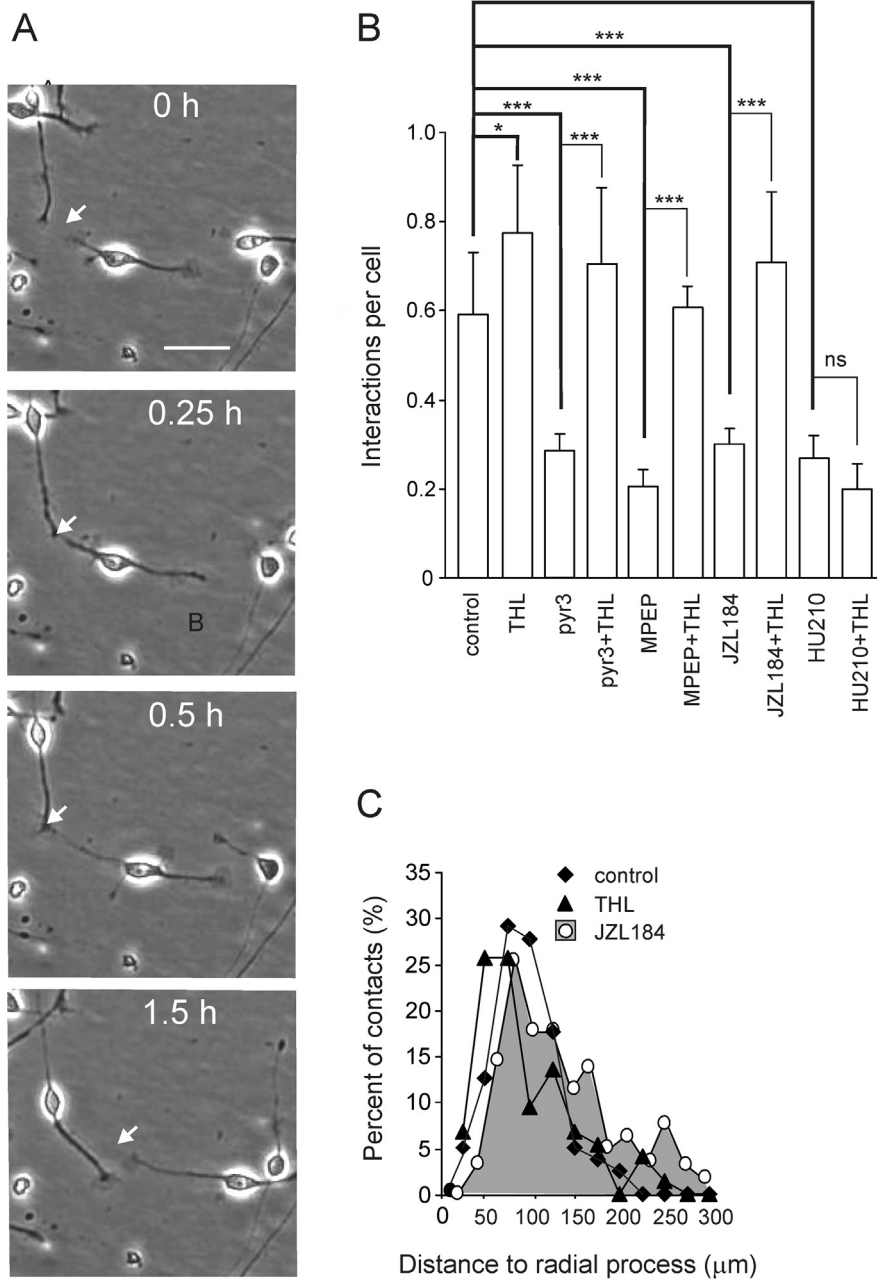
A

B

C

Fig. 6. The role of 2-AG in neuron–neuron contact. (A) Selected images from a time-lapse series demonstrating a contact between two neuroblasts. Scale bar = 50 μm. (B) Images of every 2.5-h time point were analyzed for a time period of 25 h beginning at 25 h from the start of the experiment. Each contact was counted and the number divided by the total number of neuroblasts in the respective image. Control cells ($n = 10$), and cells treated with THL (1 μM; $n = 5$), pyr3 (1 μM; $n = 5$), pyr3 + THL ($n = 5$), MPEP (10 μM; $n = 5$) JZL184 (10 μM; $n = 5$), JZL184 + THL ($n = 5$), HU-210 (1 μM; $n = 5$), and HU-210 + THL ($n = 5$). (C) Distribution of neuron–neuron contact points from the closest radial glial process. Sample sizes: control: $n = 78$; THL: $n = 73$; and JZL184: $n = 83$. Scale bar = 50 μm.

neuregulin-1 (NRG1) treatment downregulates MAGL expression leading to enhanced 2-AG signaling (Du et al., 2013).

To study the role of NRG/ErbB4, we measured the effect of NRG1 on neuronal motility. NRG1 alone caused a small but significant reduction in motility index (Fig. 7A). In contrast, when the cells were treated with

afatinib, a blocker of ErbB1/ErbB4 receptors, a considerable increase in motility was observed (Fig. 7B), similar to the effect of mGluR5, TRPC3 or MAGL inhibition (Fig. 2B, D and E; Fig. 7C). Gefitinib, a selective inhibitor of ErbB1, had no effect on the motility index (Fig. 7B), suggesting that ErbB4 mediates the effects of NRG1 and afatinib on motility. THL reversed the afatinib-induced increase in motility (Fig. 7B). NRG1, however, completely blocked the increased motility induced by JZL184 (Fig. 7C).

BDNF-treatment also increased the motility index of these cells. Interestingly, THL-treatment did not affect BDNF-induced motility (Fig. 7A). BDNF-stimulated motility instead was fully inhibited by NRG1.

DISCUSSION

The results of the present study indicate that endogenously produced 2-AG has significant impact on the motility pattern of subventricular embryonic neurosphere-derived neuronal precursor cells. Neuroblasts from this area have been shown to develop into cortical glutamatergic neurons (Kriegstein and Noctor, 2004). The endocannabinoid system has previously been shown to have an important role in cortical neuronal migration. Interference with endocannabinoid signaling by receptor knock-down or pharmacologic inhibition causes pyramidal cell migration defects and cortical malformations (Mulder et al., 2008; Saez et al., 2014; Diaz-Alonso et al., 2017). Migratory defects have also been seen upon knocking down or pharmacologically blocking of DAGL or MAGL (reviewed in Maccarrone et al., 2014).

Time-lapse microscopy was used in this study to monitor the motility pattern of cortical embryonic neurosphere-derived neuronal cells. Two cell types dominate in these neurosphere cultures, radial glial-type cells and early neurons or neuroblasts. As shown here, the CB_1 cannabinoid receptor was mainly present in neuroblasts, based on its expression in MAP-2-positive cells and the fact that little or no expression was seen in ErbB1-positive radial glial-type cells. This is supported by the data from mouse transcriptome (La Manno et al., 2016) analyses indicating that
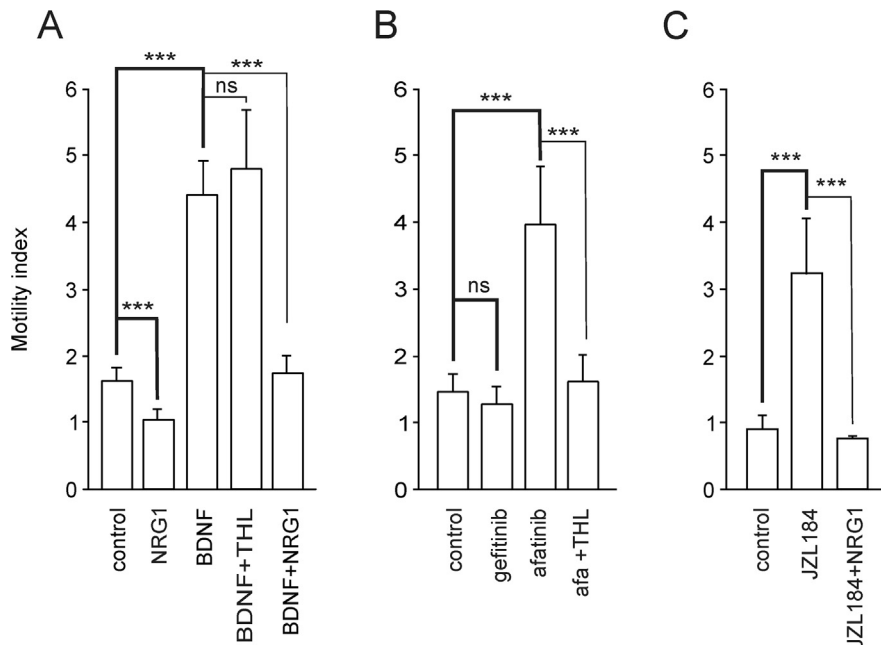
Fig. 7. The role of NRG1/ErbB4 signaling in 2-AG-mediated motility. Experimental conditions as in Fig. 2. (A) The cells were treated with NRG1 (20 nM; $n = 81$, $N = 18$), BDNF (20 ng/ml; $n = 21$, $N = 4$), BDNF + THL (1 μM; $n = 43$, $N = 7$) and BDNF + NRG1 ($n = 22$, $N = 4$). (B) The cells were treated with gefitinib (4 μM; $n = 54$, $N = 6$), afatinib (0.1 μM; $n = 71$, $N = 12$) and afatinib + THL (0.1 μM + 1μM; $n = 25$, $N = 4$) respectively. (C) The cells treated with JZL184 (10 μM; $n = 65$, $N = 9$) and JZL184 + NRG1 ($n = 12$, $N = 3$).

that CB_1 mRNA is present in neuroblasts, whereas little expression is seen in radial glia (Fig. 8).

Several parameters expected to affect the neuronal motility pattern such as turning frequency and cell–cell interaction were analyzed in this study. The neuroblasts move in phases of high motility with intermittent slow phases or stalling periods. During bursts of movement the neuroblasts show a typical bipolar morphology, while during stalling they often extend several processes (i.e., have a multipolar appearance) and rotate slowly (Tabata and Nakajima, 2003; Jansson et al., 2013; Kitazawa et al., 2014; Louhivuori et al., 2015). Studies done *in vivo* suggest that stalling phases in NPC migration represent periods of exploration and interactions (Gomez and Spitzer, 1999).

As shown here, blocking MAGL with JZL184 significantly increased endogenous 2-AG production, indicating that under basal conditions there is an intrinsic activation of 2-AG production, which is limited by the endogenous MAGL activity. The increased 2-AG levels in the presence of JZL184 caused an increase in the frequency of bursts of rapid movement of neuroblasts, reduction in their turning frequency and reduction in the cell–cell interaction frequency. These effects are in line with earlier studies on the role of MAGL in many neuronal systems, including *in vivo* mouse and rat brain, where JZL184 has been shown to increase 2-AG production and promote native endocannabinoid actions (Keimpema et al., 2010; Oudin et al., 2011a; reviewed in Oudin et al., 2011b; Maccarrone et al., 2014). Corresponding increase in neuroblast motility was obtained upon exposure to the syn-

thetic CB_1 receptor agonist HU-210, which is in agreement with previous findings with adult neuronal progenitor cells. Conversely the effect of blocking endogenous production of 2-AG with the DAGL inhibitor, THL, had a rather modest effect on the parameters analyzed. This would indicate that a tonic production of 2-AG exists, but net production is limited by a high MAGL activity and can only be unmasked by JZL184. Unfortunately, with antibodies available we were unable to identify the cells expressing DAGL and MAGL. Mouse transcriptome analysis revealed, however, that these enzymes are expressed at similar low levels in both radial glia and neuroblasts (Fig. 8).

We have previously shown that blocking of the glutamate receptor mGluR5 or the nonselective cation channel TRPC3 with pyr3, or deletion of the *trpc3* gene (Louhivuori et al., 2015), produces an increase in neuroblast motility in a similar way as did the activation of CB_1 receptors in the current study. Interestingly, this increase was totally restored to control levels when 2-AG production was blocked by THL, suggesting a functional coupling between mGluR5/TRPC3 and eCB systems. The effect of THL on motility does not appear to be a general effect on motility *per se*, since the motility increase in the presence of CB_1 receptor agonist HU-210 and BDNF were unaffected by THL treatment. The mechanisms, by which the interference with mGluR5/TRPC3 would couple to enhance endocannabinoid signaling, are uncertain. Unfortunately, the present measurement technique did not reveal any increase in the production of 2-AG in the presence of MPEP (data not shown). One explanation could be that the relevant 2-AG production is localized, and represents only a small proportion of the bulk production of 2-AG we are able to measure. Alternatively, radial glial mGluR5 signaling may affect the neuronal CB_1 receptors in some other way, possibly via diffusible substance such as NRG reducing their sensitivity (see below).

DAGL is a Ca^{2+}-activated enzyme and mGluR5 signaling can produce the DAG needed for DAGLα-catalyzed production of 2-AG in mature synapses (reviewed in Kano et al., 2009). The apparent contradictory results presented here, however, suggest that blocking of mGluR5 signaling promotes CB_1-mediated effects on migration. Stimulation of 2-AG production by DHPG, an agonist of mGluR5, was observed also in this study, but this effect was not potentiated by JZL184. One explanation could be a compartmentalization of 2-AG production and degradation, e.g., that different, separately regulated pools of 2-AG may exist. This may be related to the observations of compartmentalization of DAGL
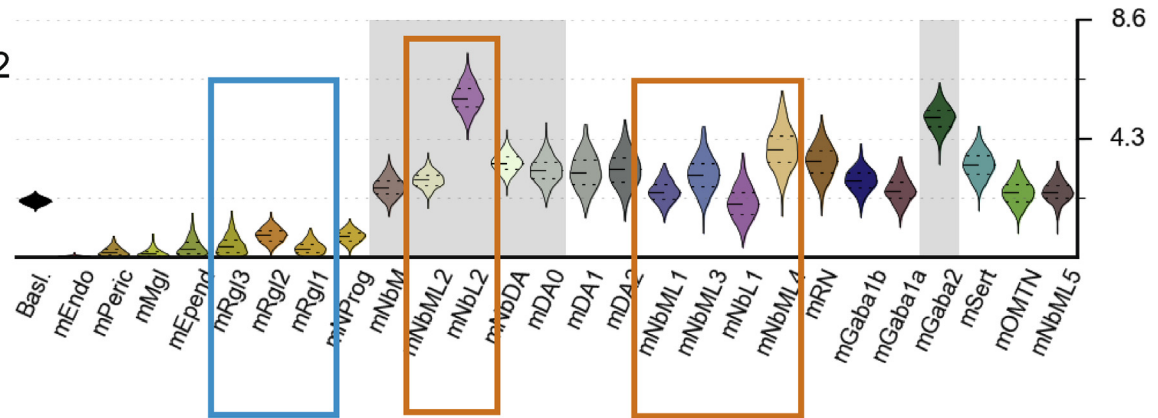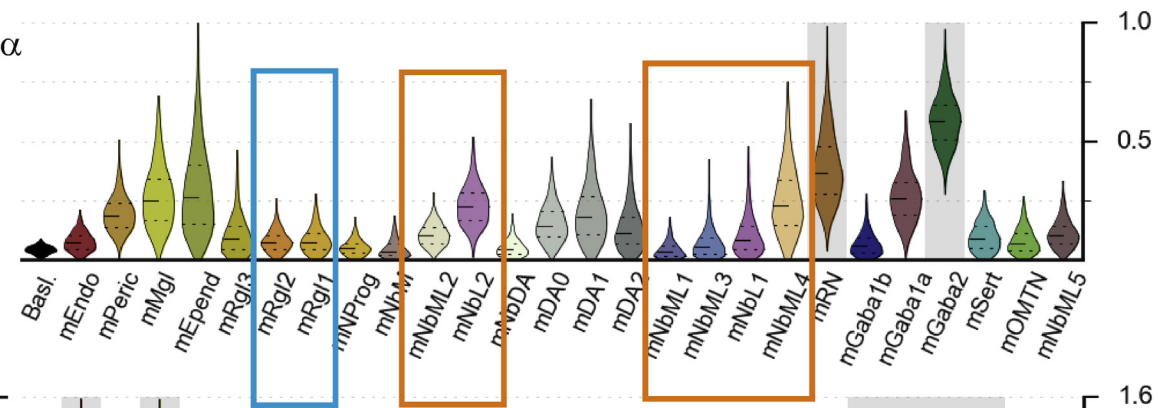
A

B
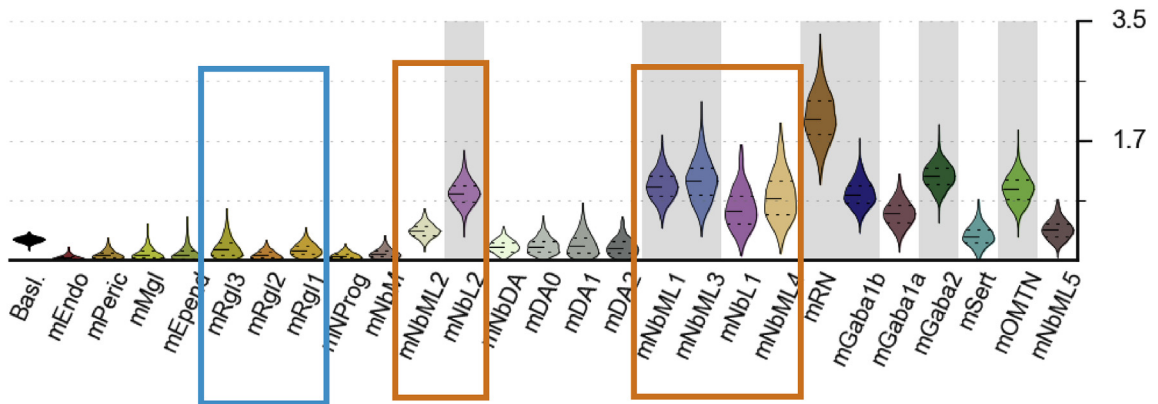
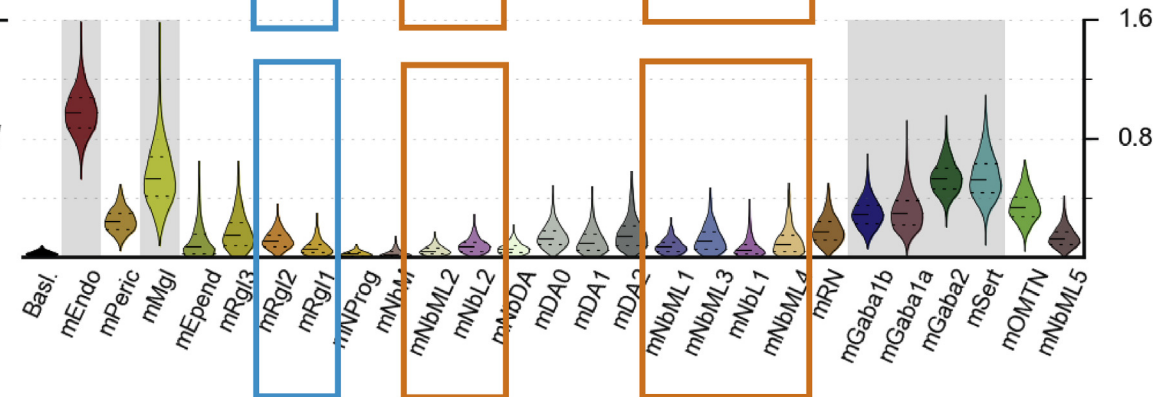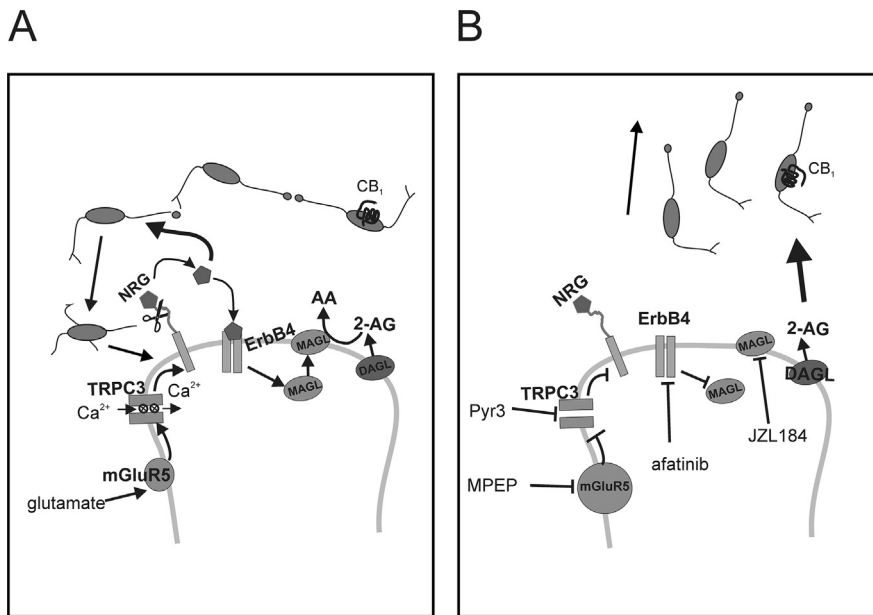**Fig. 9.** Simplified scheme to describe presented results. (A) Glutamate released from neurons acting on radial glial mGluR5 (Jansson et al., 2013; Jansson and Akerman, 2014) leads to activation of TRPC3 channels (Jansson et al., 2013; Louhivuori et al., 2015) causing a proteolytic release of membrane bound NRG (Louhivuori et al., 2018). This promotes stalling of nearby neurons via NRG activating ErbB4. NRG could also upregulates radial glial (?) MAGL, which hydrolyzes 2-AG produced by nearby DAGL (Du et al., 2013). Lack of net 2-AG production allows neuron–neuron communication. (B) Inhibition of mGluR5, TRPC3, ErbB4 or MAGL increases 2-AG production due to reduced MAGL activity, which reduces neuron–neuron contacts and promotes neuronal motility. It should be noted that the site at which different interactions occur is not certain. DAGL, MAGL and ErbB4 are also present in neurons.

may act downstream of mGluR5/TRPC3, which acts via proteolytic activation of NRG1 (Louhivuori et al., 2018). As shown here, blocking ErbB4 signaling with afatinib increased motility of neurons, in a similar way as inhibiting mGluR5/TRPC3 or MAGL or stimulating CB_1 receptors with HU-210 did. A connection between the NRG/ErbB4 system and 2-AG appears to exist, as the effect of afatinib on neuroblast motility was reversed by THL and the effect of JZL184 was reversed by NRG1. However, NRG1 treatment, contrary to THL, was able to block also the BDNF-promoted motility. We thus cannot directly pinpoint the molecular interaction between the NRG1 and endocannabinoid systems, but it seems clear that NRG1 affects neuroblast motility also by other mechanisms than by regulating MAGL expression.

Attraction between cells has previously been shown to limit the migration and positioning of transplanted neural progenitor cells (Ladewig et al., 2014). Ligands, which increase neuronal motility such as cannabinoids and MPEP, are well tolerated in clinical trials and they could thus be used as adjuncts in neural progenitor cells transplantations to enhance migration of grafted cells into the host tissue target area. In light of the results presented here, the main effect of 2-AG appears to be to counteract the attraction between neurons, thereby promoting movement for longer distances. The motility of neuroblasts is limited by two steps. First one is the neuron–radial glia attraction which promotes stalling. Second is the intense formation of neuron–neuron contacts, which also limits motility and migration distances. Interaction of neuroblasts with radial glial cells has previously been shown to limit motility by promoting stalling (Louhivuori et al., 2015). It has previously been shown that radial glia has a considerable impact on neuronal migration (Sild and Ruthazer, 2011). The reduced stalling associated with inhibition of mGluR5/TRPC3 signaling is partially caused by disturbing neuroblast–radial glial interactions (Jansson et al., 2013; Louhivuori et al., 2015). However, even if eCBs appear to be involved in the increased motility seen as a consequence of interference with mGluR5/TRPC3, the eCB effect does not involve neuron–radial glial interaction, since THL did not totally

and MAGL in neuronal processes (Keimpema et al., 2010; reviewed in Maccarrone et al., 2014). Additionally, different pools of DAGL may also exist. Two separate pools of DAGLα, one activated by metabotropic glutamate receptors and the other by Ca^{2+}, have been described in hippocampal CA1-neurons (Zhang et al., 2011). It is therefore possible that separate pools of DAGLs also exist in the neurosphere system, one that is closely connected to MAGL and another, an unconnected one. The very low mRNA expression of DAGL and MAGL in radial glia and neuroblasts supports the idea that their expression may be local. Simultaneous inhibition and stimulation of 2-AG synthesis could also represent a feed-back control on 2-AG production.

Less is known about the regulation of the 2-AG-degrading enzyme, MAGL. Its expression has been shown to be activated through peroxisome proliferator-activated receptor-γ (PPARγ) (Labar et al., 2010). Neurotrophins might also have a role in the regulation the of 2-AG tone. BDNF/TrkB signaling has been shown to downregulate MAGL expression (Maison et al., 2009) and, interestingly, there is evidence for involvement of NRG1 in upregulation of MAGL (Du et al., 2013). NRG1

Fig. 8. Transcriptome analysis of CB1, MAP2, DAGL and MAGL. Data from (La Manno et al., 2016). CB_1: In mouse (bottom panel) significant expression in neuroblasts on contrary to radial glia cells, where the expression is low. MAP2: expression is seen exclusively in neuroblasts. DAGL: Expressed in both cell types in low amounts compared to baseline. MAGL: Expressed in both cell types in low amounts compared to baseline. Abbreviations: mRgl1 = mouse radial glia 1, 2, and 3 cell type (blue rectangle). mNbML = mouse neuroblast Mediolateral (orange rectangle). mNbL = mouse neuroblast lateral (orange rectangle). mNProg = mouse neural progenitor. note: neuroblast is a dividing cell that will develop into a neuron after migration phase (i.e., intermediate progenitor). neural progenitor: Close to a stem cell (identified by expression of Msx2, found only in floor plate of midbrain).

reverse the reduced neuron–radial glial attraction, but promoted stalling and positioning of neurons closer (100–200 µm) to the radial glial processes. Most of the neuron–neuron interactions occur at this distance. THL enhanced neuron–neuron contacts, particularly when contacts were first reduced by blocking of mGluR5/TRPC3 or in the presence of JZL184. Endocannabinoids thus appear to reduce neuron–neuron interactions. This is supported by the findings of Diaz-Alonzo and coworkers where transient CB_1 knockdown induced disruption in migratory morphology and arrest in migration (Diaz-Alonso et al., 2017). eCBs have previously been shown to cause growth cone repulsion (Berghuis et al., 2007; Argaw et al., 2011; reviewed in Maccarrone et al., 2014), which would explain the increased number of neuron–neuron contacts upon inhibition of eCB synthesis. Transient early neuron–neuron attraction is considered to be an important step in future synaptogenesis (Cao et al., 2009). Reduced neuron–neuron interaction might alter correct positioning of neurons during brain development (reviewed in Maccarrone et al., 2014; Zhou et al., 2014).

CONCLUSION

The results presented suggest that attraction between neuroblasts is an important factor limiting the progress of early neuronal movement. Local intrinsic DAGL-mediated eCB production is limited by MAGL-mediated hydrolysis. Radial glial mGluR5, acting via TRPC3 channels, promote the production diffusible signals – NRG acting on ErbB4 probably being one of them – which may reduce the net production of eCBs and/or reduce neuronal CB_1 receptor sensitivity to eCBs. Lack of eCB production (or CB_1 activation) reverses eCB-mediated inhibition of neuron–neuron interaction leading to an increased motility and longer distances of movement. Schematic picture of the possible signaling involved is shown in Fig. 9.

ACKNOWLEDGMENTS

REFERENCES

Amaral MD, Pozzo-Miller L (2007) TRPC3 channels are necessary for brain-derived neurotrophic factor to activate a nonselective cationic current and to induce dendritic spine formation. J Neurosci 27:5179–5189.

Argaw A, Duff G, Zabouri N, Cecyre B, Chaine N, Cherif H, et al. (2011) Concerted action of CB1 cannabinoid receptor and deleted in colorectal cancer in axon guidance. J Neurosci 31:1489–1499.

Berg AP, Sen N, Bayliss DA (2007) TrpC3/C7 and Slo2.1 are molecular targets for metabotropic glutamate receptor signaling in rat striatal cholinergic interneurons. J Neurosci 27:8845–8856.

Berghuis P, Rajnicek AM, Morozov YM, Ross RA, Mulder J, Urban GM, et al. (2007) Hardwiring the brain: endocannabinoids shape neuronal connectivity. Science 316:1212–1216.

Bisogno T, Howell F, Williams G, Minassi A, Cascio MG, Ligresti A, et al. (2003) Cloning of the first sn1-DAG lipases points to the spatial and temporal regulation of endocannabinoid signaling in the brain. J Cell Biol 163:463–468.

Brazel CY, Nunez JL, Yang Z, Levison SW (2005) Glutamate enhances survival and proliferation of neural progenitors derived from the subventricular zone. Neuroscience 131:55–65.

Cao D, Kevala K, Kim J, Moon HS, Jun SB, Lovinger D, et al. (2009) Docosahexaenoic acid promotes hippocampal neuronal development and synaptic function. J Neurochem 111:510–521.

Devane WA, Hanus L, Breuer A, Pertwee RG, Stevenson LA, Griffin G, et al. (1992) Isolation and structure of a brain constituent that binds to the cannabinoid receptor. Science 258:1946–1949.

Di Giorgi Gerevini VD, Caruso A, Cappuccio I, Ricci Vitiani L, Romeo S, Della Rocca C, et al. (2004) The mGlu5 metabotropic glutamate receptor is expressed in zones of active neurogenesis of the embryonic and postnatal brain. Brain Res Dev Brain Res 150:17–22.

Di Marzo V (2011) Endocannabinoid signaling in the brain: biosynthetic mechanisms in the limelight. Nat Neurosci 14:9–15.

Diaz-Alonso J, de Salas-Quiroga A, Paraiso-Luna J, Garcia-Rincon D, Garcez PP, Parsons M, et al. (2017) Loss of cannabinoid CB1 receptors induces cortical migration malformations and increases seizure susceptibility. Cereb Cortex 27:5303–5317.

Du H, Kwon IK, Kim J (2013) Neuregulin-1 impairs the long-term depression of hippocampal inhibitory synapses by facilitating the degradation of endocannabinoid 2-AG. J Neurosci 33:15022–15031.

Galve-Roperh I, Palazuelos J, Aguado T, Guzman M (2009) The endocannabinoid system and the regulation of neural development: potential implications in psychiatric disorders. Eur Arch Psychiatry Clin Neurosci 259:371–382.

Gandhi R, Luk KC, Rymar VV, Sadikot AF (2008) Group I mGluR5 metabotropic glutamate receptors regulate proliferation of neuronal progenitors in specific forebrain developmental domains. J Neurochem 104:155–172.

Gao Y, Vasilyev DV, Goncalves MB, Howell FV, Hobbs C, Reisenberg M, et al. (2010) Loss of retrograde endocannabinoid signaling and reduced adult neurogenesis in diacylglycerol lipase knock-out mice. J Neurosci 30:2017–2024.

Ghashghaei HT, Weber J, Pevny L, Schmid R, Schwab MH, Lloyd KC, et al. (2006) The role of neuregulin-ErbB4 interactions on the proliferation and organization of cells in the subventricular zone. Proc Natl Acad Sci U S A 103:1930–1935.

Gomez TM, Spitzer NC (1999) In vivo regulation of axon extension and pathfinding by growth-cone calcium transients. Nature 397:350–355.

Jansson LC, Akerman KE (2014) The role of glutamate and its receptors in the proliferation, migration, differentiation and survival of neural progenitor cells. J Neural Transm (Vienna) 121:819–836.

Jansson LC, Louhivuori L, Wigren HK, Nordstrom T, Louhivuori V, Castren ML, et al. (2012) Brain-derived neurotrophic factor increases the motility of a particular N-methyl-D-aspartate / GABA-responsive subset of neural progenitor cells. Neuroscience 224:223–234.

Jansson LC, Louhivuori L, Wigren HK, Nordstrom T, Louhivuori V, Castren ML, et al. (2013) Effect of glutamate receptor antagonists on migrating neural progenitor cells. Eur J Neurosci 37:1369–1382.

Kano M, Ohno-Shosaku T, Hashimotodani Y, Uchigashima M, Watanabe M (2009) Endocannabinoid-mediated control of synaptic transmission. Physiol Rev 89:309–380.

Keimpema E, Barabas K, Morozov YM, Tortoriello G, Torii M, Cameron G, et al. (2010) Differential subcellular recruitment of

monoacylglycerol lipase generates spatial specificity of 2-arachidonoyl glycerol signaling during axonal pathfinding. J Neurosci 30:13992–14007.

Keimpema E, Mackie K, Harkany T (2011) Molecular model of cannabis sensitivity in developing neuronal circuits. Trends Pharmacol Sci 32:551–561.

Kim SJ, Kim YS, Yuan JP, Petralia RS, Worley PF, Linden DJ (2003) Activation of the TRPC1 cation channel by metabotropic glutamate receptor mGluR1. Nature 426:285–291.

Kitazawa A, Kubo K, Hayashi K, Matsunaga Y, Ishii K, Nakajima K (2014) Hippocampal pyramidal neurons switch from a multipolar migration mode to a novel ''climbing'' migration mode during development. J Neurosci 34:1115–1126.

Kriegstein AR, Noctor SC (2004) Patterns of neuronal migration in the embryonic cortex. Trends Neurosci 27:392–399.

La Manno G, Gyllborg D, Codeluppi S, Nishimura K, Salto C, Zeisel A, et al. (2016) Molecular diversity of midbrain development in mouse, human, and stem cells. Cell 167(566–580):e519.

Labar G, Wouters J, Lambert DM (2010) A review on the monoacylglycerol lipase: at the interface between fat and endocannabinoid signalling. Curr Med Chem 17:2588–2607.

Ladewig J, Koch P, Brustle O (2014) Auto-attraction of neural precursors and their neuronal progeny impairs neuronal migration. Nat Neurosci 17:24–26.

Li HS, Xu XZ, Montell C (1999) Activation of a TRPC3-dependent cation current through the neurotrophin BDNF. Neuron 24:261–273.

Louhivuori LM, Jansson L, Turunen PM, Jantti MH, Nordstrom T, Louhivuori V, et al. (2015) Transient receptor potential channels and their role in modulating radial glial-neuronal interaction: a signaling pathway involving mGluR5. Stem Cells Dev 24:701–713.

Louhivuori LM, Turunen PM, Louhivuori V, Yellapragada V, Nordstrom T, Uhlen P, et al. (2018) Regulation of radial glial process growth by glutamate via mGluR5/TRPC3 and neuregulin/ErbB4. Glia 66:94–107.

Maccarrone M, Guzman M, Mackie K, Doherty P, Harkany T (2014) Programming of neural cells by (endo)cannabinoids: from physiological rules to emerging therapies. Nat Rev Neurosci 15:786–801.

Maison P, Walker DJ, Walsh FS, Williams G, Doherty P (2009) BDNF regulates neuronal sensitivity to endocannabinoids. Neurosci Lett 467:90–94.

Marin O, Valiente M, Ge X, Tsai LH (2010) Guiding neuronal cell migrations. Cold Spring Harb Perspect Biol 2:a001834.

Meijering E, Dzyubachyk O, Smal I (2012) Methods for cell and particle tracking. Methods Enzymol 504:183–200.

Mulder J, Aguado T, Keimpema E, Barabas K, Ballester Rosado CJ, Nguyen L, et al. (2008) Endocannabinoid signaling controls pyramidal cell specification and long-range axon patterning. Proc Natl Acad Sci U S A 105:8760–8765.

Murase S, Horwitz AF (2002) Deleted in colorectal carcinoma and differentially expressed integrins mediate the directional migration of neural precursors in the rostral migratory stream. J Neurosci 22:3568–3579.

Nguyen L, Rigo JM, Rocher V, Belachew S, Malgrange B, Rogister B, et al. (2001) Neurotransmitters as early signals for central nervous system development. Cell Tissue Res 305:187–202.

Oudin MJ, Gajendra S, Williams G, Hobbs C, Lalli G, Doherty P (2011a) Endocannabinoids regulate the migration of subventricular zone-derived neuroblasts in the postnatal brain. J Neurosci 31:4000–4011.

Oudin MJ, Hobbs C, Doherty P (2011b) DAGL-dependent endocannabinoid signalling: roles in axonal pathfinding, synaptic plasticity and adult neurogenesis. Eur J Neurosci 34:1634–1646.

Rakic P, Ayoub AE, Breunig JJ, Dominguez MH (2009) Decision by division: making cortical maps. Trends Neurosci 32:291–301.

Rao Y, Wong K, Ward M, Jurgensen C, Wu JY (2002) Neuronal migration and molecular conservation with leukocyte chemotaxis. Genes Dev 16:2973–2984.

Reynolds BA, Weiss S (1992) Generation of neurons and astrocytes from isolated cells of the adult mammalian central nervous system. Science 255:1707–1710.

Rico B, Marin O (2011) Neuregulin signaling, cortical circuitry development and schizophrenia. Curr Opin Genet Dev 21:262–270.

Saez TM, Aronne MP, Caltana L, Brusco AH (2014) Prenatal exposure to the CB1 and CB2 cannabinoid receptor agonist WIN 55,212–2 alters migration of early-born glutamatergic neurons and GABAergic interneurons in the rat cerebral cortex. J Neurochem 129:637–648.

Savinainen JR, Saario SM, Laitinen JT (2012) The serine hydrolases MAGL, ABHD6 and ABHD12 as guardians of 2-arachidonoylglycerol signalling through cannabinoid receptors. Acta Physiol (Oxf) 204:267–276.

Schneider CA, Rasband WS, Eliceiri KW (2012) NIH Image to ImageJ: 25 years of image analysis. Nat Methods 9:671–675.

Sild M, Ruthazer ES (2011) Radial glia: progenitor, pathway, and partner. Neuroscientist 17:288–302.

Suzuki SO, Goldman JE (2003) Multiple cell populations in the early postnatal subventricular zone take distinct migratory pathways: a dynamic study of glial and neuronal progenitor migration. J Neurosci 23:4240–4250.

Tabata H, Nakajima K (2003) Multipolar migration: the third mode of radial neuronal migration in the developing cerebral cortex. J Neurosci 23:9996–10001.

Tanimura A, Yamazaki M, Hashimotodani Y, Uchigashima M, Kawata S, Abe M, et al. (2010) The endocannabinoid 2-arachidonoylglycerol produced by diacylglycerol lipase alpha mediates retrograde suppression of synaptic transmission. Neuron 65:320–327.

Turunen PM, Jantti MH, Kukkonen JP (2012) OX1 orexin/hypocretin receptor signaling through arachidonic acid and endocannabinoid release. Mol Pharmacol 82:156–167.

Zhang L, Wang M, Bisogno T, Di Marzo V, Alger BE (2011) Endocannabinoids generated by Ca2+ or by metabotropic glutamate receptors appear to arise from different pools of diacylglycerol lipase. PLoS ONE 6:e16305.

Zhao L, Jiao Q, Huang C, Hou N, Chen X, Zhang J, et al. (2014) MGluR5 promotes the differentiation of rat neural progenitor cells into cholinergic neurons and activation of extracellular signal-related protein kinases. NeuroReport 25:427–434.

Zhou Y, Falenta K, Lalli G (2014) Endocannabinoid signalling in neuronal migration. Int J Biochem Cell Biol 47:104–108.

Zhou Y, Oudin MJ, Gajendra S, Sonego M, Falenta K, Williams G, et al. (2015) Regional effects of endocannabinoid, BDNF and FGF receptor signalling on neuroblast motility and guidance along the rostral migratory stream. Mol Cell Neurosci 64:32–43.

GLOSSARY

Neurosphere: A culture system of free-floating aggregate of neural stem cells.

Motility index: A parameter describing the phasic nature of neuronal precursor movement; higher motility index means more movement (defined as number of time points the cells move with a speed above 30 μm/h divided by the number of time points they move below this value).

APPENDIX A. SUPPLEMENTARY DATA

Supplementary data associated with this article can be found, in the online version, at https://doi.org/10.1016/j.neuroscience.2018.02.005.